RSC Advances

PAPER

View Article Online
View Journal | View Issue

Cite this: *RSC Adv.*, 2022, **12**, 5807

Large refractive index changes in ZIF-8 thin films of optical quality†

Nils Christian Keppler, [ab] Karen Deli Josephine Hindricks [ab] and Peter Behrens *[ab]

Received 21st November 2021
Accepted 9th February 2022

DOI: 10.1039/d1ra08531j

rsc.li/rsc-advances

ZIF-8 (zeolitic imidazolate framework-8) is a member of the growing family of metal–organic frameworks (MOFs). Homogeneous and crack-free ZIF-8 thin films of optical quality were crystallized on silicon and glass substrates. The refractive index of such ZIF-8 thin films in the complete visible light spectrum was directly determined for the first time. By incubating the porous films in different substances, the refractive index could be modulated over a wide range, two times larger than previously reported for MOF thin films. Reversible refractive index switching in ZIF-8 thin films was performed *via* the liquid and the gas phase. The ability to adjust the refractive index over a broad range enables the use of ZIF-8 films for applications in optical devices such as sensors, coatings for mirrors and lenses, or as an optical medium in more complex optical devices.

1. Introduction

Optical systems are important for many devices in our daily lives. For many optical applications, refractive index modulators are important, *e.g.* in sensors,[1] optical data storage[2] and optical fiber communication.[3] Changes in the refractive index of a material can for example be initiated by photostimulation[2,4] but also by applying an electric field[3,5] (electrooptical Pockels and Kerr effects) or other external stimuli. To enable the use of optical systems in a broader range of devices, novel types of systems are of interest, for example by using stacks of layers with different optical activities, replacing traditional optical systems like mirrors and lenses made from glass.[6] Such constructs may enable the fabrication of, *e.g.*, highly compact lab-on-a-chip (LOC)[7] devices with integrated miniaturized mirrors, lenses and filters.[6,7] Modern fabrication techniques like additive manufacturing will allow the production of such devices at much lower costs and will foster their widespread distribution. However, novel materials with higher degrees of functionality will be necessary in order to generate various features in such miniaturized devices. For example, refractive index changes are limited in many traditional materials.[2,4,5] Modern porous materials like metal–organic frameworks are able to open up new pathways for reversible refractive index modulation, for example by the adsorption of molecules.

Metal–organic frameworks (MOFs) are a class of highly porous hybrid materials. They consist of inorganic building units (IBUs) that are interconnected by organic linker molecules.[8] The freedom to choose different inorganic building units (IBUs) and linker molecules with different lengths and functionalities makes MOFs an interesting material class for different traditional applications of porous solids like sensing,[9,10] catalysis,[11,12] gas storage[13–15] and gas separation.[16–18] Apart from these traditional applications, MOFs can also be used beneficially in other fields, like electronics, optoelectronics and optics.[19–22]

The refractive index as a basic inherent optical property of MOFs has been largely overlooked for quite some time; only in the last few years, the interest in the evaluation of the refractive index of MOFs has increased somewhat.[23,24] Time-resolved[25–29] or non-time-resolved[30–32] changes in the refractive index of MOFs have been directly measured, in most cases *via* ellipsometry. For such measurements, thin MOF films of optical quality are necessary. Tao *et al.*[23,24,31] have fabricated MOF thin films by coating from nanoparticle dispersions, showing the influence of the coating methods, of the functionalizations of the linker molecules, and of postsynthetic modifications on the refractive index of nanoparticulate MOF thin films. One of their main findings is that voids between the nanoparticles influence the refractive index of the resulting films. Demessence[27] and Dalstein[28] used thin films prepared from ZIF-8 nanoparticles for isopropanol or styrene sensing, achieving refractive index changes of $\Delta n = 0.08$ for isopropanol and $\Delta n = 0.05$ for styrene. ZIF-8-coated optical fibers were used by Vandezande[25] and Kim[26] to realize sensing of *n*-butanol or carbon dioxide. Refractive index changes of $\Delta n = 0.06$ for *n*-butanol and $\Delta n = 0.005$ for CO_2 were reported. Redel[30] prepared HKUST-1 thin

[a]*Institute for Inorganic Chemistry, Leibniz Universität Hannover, Hannover, Germany. E-mail: peter.behrens@acb.uni-hannover.de*

[b]*Cluster of Excellence PhoenixD (Photonics, Optics and Engineering – Innovation across Disciplines), Leibniz Universität Hannover, Hannover, Germany*

† Electronic supplementary information (ESI) available. See DOI: 10.1039/d1ra08531j

films using a layer-by-layer method and tuned its refractive index by $\Delta n = 0.1$, changing between the activated (empty) and the ethanol-loaded state of the film. In most of these cases, the changes in the refractive index have been explained by a pore-filling effect, caused by gas sorption.[32,33] An overview over these experiments shows that, until now, $\Delta n = 0.1$ is the limit for directly measured refractive index changes of metal–organic frameworks.

In addition, changes in optical spectra have also been associated with changes in the refractive index of metal–organic frameworks.[34–37] MOFs were used, for example, for the construction of 3D photonic crystals of HKUST-1 (ref. 34) which showed shifts in the UV/Vis spectra after the adsorption of molecules like ethanol, acetone, cyclohexane and toluene. Also gratings produced from spin-crossover MOFs[35] and MOF-coated colloidal monolayers[36] show shifts in their optical spectra under external stimuli. Hupp and co-workers[37] detected propane in nitrogen atmosphere and ethanol in water with ZIF-8 thin films by variations in the transmission spectra of these films. These examples show that the evaluation of the refractive indices of metal–organic frameworks is an important topic for the use of MOFs in optical technologies and optical sensors.

Zeolitic imidazolate frameworks (ZIFs) are MOFs with zeolite-analogue structures which have high thermal and chemical stabilities.[38] ZIF-8 is one of the most prominent ZIFs, consisting of zinc ions that are bridged by 2-methylimidazolate linkers, forming a crystalline framework with sod topology. It has been widely studied[39–41] and characterized.[18,42] Here, we use ZIF-8 thin films as a host structure for the loading with different substances to fine-tune the refractive index of this material and also to work towards large refractive index changes. The basis for this approach is the wide refractive index range of organic substances.[43,44] Adjustable refractive indices could enable applications in optical devices, *e.g.* in lense and mirror coatings, for sensors, in waveguiding elements, optical filters or in Fabry–Pérot devices.[37,45] We have fabricated thin films of ZIF-8 of optical quality on different substrates, have measured their refractive index using ellipsometry, and have changed the refractive index by sorption of different organic molecules.

2. Materials and methods

2.1 Materials

$Zn(NO_3)_2 \cdot 6H_2O$ (98%, Sigma-Aldrich), 2-methylimidazole (99%, Sigma-Aldrich), methanol (99.5%, Roth), ethanol (99.8%, Fisher-Scientific), tetrahydrofurane (99.5%, Roth), dimethylformamide (99.8%, Sigma-Aldrich), dimethylsulfoxide (99.9%, Sigma-Aldrich), toluene (99.9%, Roth), *para*-methyl anisate (98%, Alfa-Aesar), iodobenzene (98%, Alfa-Aesar), sulfuric acid (96%, Roth) and hydrogen peroxide (35%, Roth) were used without further purification. For ^{1}H-NMR measurements, DMSO-d6 (99.8 atom % D, Acros-Organics) and DCl (20 wt% in D_2O, 99 atom % D, euriso-top) were used.

As substrates for the deposition of ZIF-8 we used silicon wafers which were cut into 1 × 1 cm pieces and glass slides cut into 2 × 2.5 cm pieces. All substrates were cleaned with ethanol and then immersed in a fresh mixture of sulfuric acid and hydrogen peroxide (2 : 1) for 15 minutes. Subsequently, they were washed with water, ethanol and methanol. Cleaned substrates were not stored but directly used.

2.2 ZIF-8 thin film and powder fabrication

ZIF-8 thin films were fabricated using the cycled direct growth method as described by Hupp *et al.*[37] with some modifications. Stock solutions of 25 mM $Zn(NO_3)_2 \cdot 6H_2O$ and 50 mM 2-methylimidazole in methanol were prepared. Cleaned substrates were incubated in a 1 : 1 volume mixture of the stock solutions (synthesis solution) at room temperature. After 30 minutes the substrates were removed, rinsed with pure methanol and directly afterwards incubated in a freshly prepared synthesis solution. This process represents a deposition cycle. For comparison, some samples were prepared with a drying step in a nitrogen stream between each deposition cycle, as described in the literature.[37]

Typically, the thin films were prepared with three deposition cycles. After the final synthesis cycle, the samples were rinsed with methanol and directly incubated in ethanol. They were left in ethanol at least over night at room temperature before being used in further experiments. Samples on silicon wafers were used for the ellipsometry and sorption measurements. Samples on glass were used for the UV/Vis and XRD measurements.

ZIF-8 powder samples were synthesized with a similar method: 100 mL of a 25 mM $Zn(NO_3)_2 \cdot 6H_2O$ solution was mixed with 100 mL 50 mM 2-methylimidazole (both in methanol) under stirring. The resulting solution was mixed for 1 h. The powder was separated *via* centrifugation, washed with ethanol twice and dried under reduced pressure at room temperature.

2.3 Refractive index tuning and switching

For the refractive index modulation experiments, ZIF-8 films that had previously been stored in ethanol were incubated in different liquid media for three days at room temperature. Afterwards, the films were dried in air for a few minutes. Ethanol, tetrahydrofurane (THF), dimethylformamide (DMF), dimethylsulfoxide (DMSO), toluene and iodobenzene were used as incubation media.

Faster refractive index modulation experiments were performed by alternating incubation of ZIF-8 thin films in toluene and ethanol for 60 minutes each. For the UV/Vis and ellipsometry studies, an ethanol-stored ZIF-8 film on glass (for UV/Vis spectroscopy) or silicon (for ellipsometry measurements) was incubated several times in toluene, each time for 10–30 min. In between, the UV/Vis or ellipsometry measurement of the sample was carried out. In an analogous fashion, a toluene-stored ZIF-8 film was incubated in ethanol for 10–30 min several times, with UV/Vis or ellipsometry measurements in between.

Gas-phase loading experiments were performed with *para*-methyl anisate (pMA). In a typical loading experiment, ethanol-soaked ZIF-8 films positioned in 3 mL glass vessels were placed in a 100 mL Schlenk flask. 100 mg *para*-methyl anisate was added. The Schlenk flask was evacuated to 1 mbar and heated in an oven at 120 °C for 2 days. Afterwards the films were shortly

washed with ethanol and dried in air for a few minutes at room temperature.

2.4 Characterization of powder samples

To determine the actual composition of the loaded samples, ^{1}H-NMR spectroscopy was carried out on digested samples. Digestion was carried out by dissolving 10 mg of ZIF-8 powder in 650 μL DMSO-d6 by addition of 15 μL DCl (2 wt% in D_2O). Dissolved thin film samples did not show any signals in the NMR spectra because digested films did not deliver enough material for detection and determination. Therefore, powder samples were treated in a similar way to investigate the loading of ZIF-8 with different molecules: typically, 20 mg ZIF-8 powder was stirred in 2 mL of the organic liquid (ethanol, toluene or iodobenzene) for 3 days. After centrifugation the samples were dried for 2 hours at room temperature on filter paper. Loading experiments with pMA were also performed. The device and the procedure used for the measurements are described below.

2.5 Characterization of thin films

XRD measurements on ZIF-8 thin films were carried out with an X-ray diffractometer from STOE working in Bragg–Brentano geometry. An Iso-Debyeflex 3003 was used for the generation of X-rays at 40 kV and 30 mA, delivering CuKα_1 radiation. Measurements were carried out between 5 and 30° 2θ with a step size of 0.01° 2θ and a measuring time of 20 s per step.

A Sentech SE800 spectroscopic ellipsometer with a spectral range from 370 to 850 nm was used for the ellipsometry measurements. All measurements were performed at angles of incidence of 50°, 60° and 70°. Ellipsometry data were fitted with a Cauchy dispersion model using the software SpectraRay 3 (Sentech). Time-resolved measurements with argon and ethanol were carried out only at 70° to enable fast measurements. More information about the fitting model is given in the ESI (Table S1†).

SEM images of coated glass slides were taken by fixing samples with carbon tape on SEM metal substrate holders. Electrical contact of the thin films was ensured by the use of silver conductive lacquer and by sputtering the samples with a thin layer of gold. SEM images were recorded with a JSM-6610L V (Joel). Images were taken at 10 kV with a working distance of 10 mm.

For the liquid ^{1}H-NMR measurements a DPX400 AvanceSpectrometer (Bruker) was used. All samples were measured at 400 MHz.

UV/Vis spectra were recorded in transmission (transmission spectra on glass) or reflection (reflection spectra on silicon wafers) with a Cary 4000 (Agilent Technologies) in a maximum spectral range from 200 to 800 nm.

AFM measurements were performed using a NX 10 by Park System Corp. Images were taken in non-contact mode with a scan rate of 0.5 Hz. The software "XEI" (5.2.0 by Park System Corp.) was used for the data analysis.

IR measurements were performed with a Tensor 27 (Bruker) in a spectral range from 4000 to 600 cm^{-1}, using an ATR setup.

Krypton physisorption isotherms were measured at 87 K on an Autosorb 1 instrument from Quantachrome and were evaluated with the software ASiQwin 2.0 (Quantachrome). Prior to the measurements, the samples were degassed under vacuum at 120 °C for 24 h. Surface areas were determined by applying the Brunauer–Emmett–Teller (BET) equation.

3. Results and discussion

For optical applications, very good optical quality of a thin film sample is highly important. Therefore, thin films need to be crack-free, transparent and homogeneous. For applications where the defined porosity of the framework is important, the films also need to be crystalline. Thin films made from nanoparticles, which normally contain voids between the particles, are usually optically inhomogeneous due to non-regular packing. Opal films are an exception, but can be problematic as well. The refractive index of such thin films is a sum of the refractive index of the nanoparticles and of the air in the voids between the particles. ZIF-8 thin films on glass and silicon which were produced by cyclic direct crystallization[37] were shown to be dense (*i.e.* free from intercrystallite voids) and homogeneous except for the problem that cracks in the films may appear, as can be identified in the cross-sectional SEM images in the referred paper.[37] Therefore, we modified the synthesis protocol described by Lu and Hupp[37] with the aim to obtain crack-free ZIF-8 thin films. Cracks may easily form when thin films are dried.[46] Drying leads to capillary and mechanical stress in the material which may result in the formation of cracks. In the reported synthesis protocol, the ZIF-8 thin films are dried in a nitrogen stream between every deposition cycle.[37] To avoid unnecessary stress, we modified the synthesis protocol and skipped these drying steps. Finally, the completely prepared films were stored in ethanol in order to avoid unprotocolled sorption/desorption events.

All prepared ZIF-8 thin films are transparent for the naked eye (Fig. S1, ESI†). On glass substrates, the films are only visible from an oblique viewing angle, due to interference colors which appear due to the thickness of the films lying in the range of light wavelengths (Fig. S2, ESI†). Transmission spectra of films prepared with three, five and eight deposition cycles (Fig. S3†) and a reflectance spectrum of a film on silicon (prepared with three deposition cycles, Fig. S4†) are given in the ESI.† These spectra underline the high transparency of the thin films.

According to XRD measurements, crystalline ZIF-8 thin films can already be obtained after two deposition cycles (Fig. 1). The crystallinity is further enhanced after three deposition cycles, but does not increase anymore thereafter (*e.g.* after five cycles, see Fig. 1). The XRD patterns are in good agreement with a calculated literature pattern of ZIF-8.[38] Results reported below always refer to thin films prepared using three deposition cycles.

In Fig. 2, SEM images show the difference between ZIF-8 thin films prepared with the original[37] and our modified method. When the films are dried between each deposition cycle, cracks are formed that cannot be filled in the following deposition cycles. When these drying steps are skipped, crack-free films are

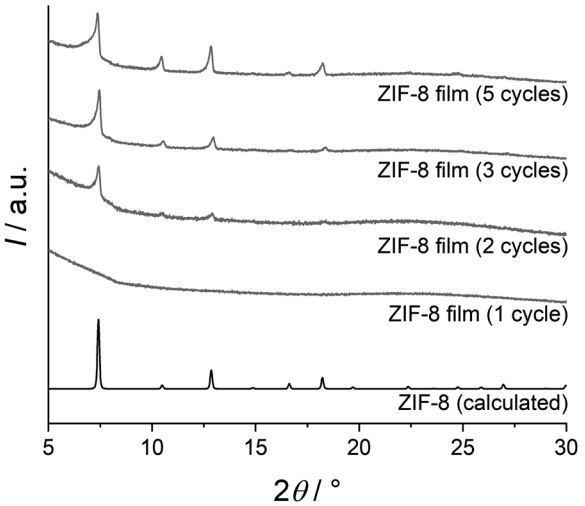

Fig. 1 XRD patterns of thin films obtained with different numbers of deposition cycles, compared with a calculated XRD pattern of ZIF-8.[38]

obtained. Furthermore, AFM measurements performed on ZIF-8 films on coated silicon wafers (prepared with three deposition cycles) confirm that the films are crack-free. The results of five measurements yield the roughness parameters $R_a = (5.21 \pm 0.17)$ nm and $R_q = (6.46 \pm 0.27)$ nm. Additional information on the AFM data is given in the ESI (Fig. S5 and S6†).

To confirm the high porosity of the ZIF-8 thin films, krypton physisorption measurements were carried out (see Fig. 3 left). The BET area increases linearly with the number of deposition cycles used in the preparation of the films (Fig. 3 right, red columns). The film deposited with three cycles shows a high porosity with a BET area of 930 $cm^2\ cm^{-2}$.

The ZIF-8 thin films were characterized in terms of their optical properties. As-synthesized thin films on silicon wafers were stored in water-free ethanol over night to remove guest molecules from the pores. The focus of the optical characterization is on the refractive index. The data for Ψ and Δ measured by ellipsometry were fitted with a Cauchy model including a roughness layer. The roughness layer is important to improve the fit to the refractive index dispersion of the ZIF-8 film. For all ellipsometry measurements the mean squared error (MSE) of the fit is below 3 (usually around 1; the MSE should always be below 3 to ensure sufficiently good agreement of the measured curves and the fitted data). A typical fit result is shown in Fig. S7 (ESI†). Also, additional information about the ellipsometry model can be found in the ESI (Table S1†). The average value for the thickness of the roughness layer is 30 nm. Compared with a histogram of an AFM measurement (ESI, Fig. S6†), the roughness value of 30 nm covers height variations across the whole sample (*i.e.* capturing nearly all pixels of the AFM measurement), so both methods are in good agreement. Nevertheless, a large number of pixels and therefore a large number of crystallites have similar heights, resulting in a lower roughness which is captured by the arithmetic mean roughness value R_a that is given above.

The average refractive index of ten samples of the ZIF-8 films is $n_D(\text{empty}) = 1.355 \pm 0.004$ at the commonly used wavelength of 589 nm (D line of sodium vapor). These samples had been stored in ethanol, but the ethanol had desorbed before the measurement. To verify this, ^{1}H-NMR spectroscopic measurements were carried out on samples treated in an analogous way with regard to storage in and removal from ethanol. The samples were digested in acidic solution before the NMR measurements. No signals could be detected on solutions based on digested thin films due to a too high dilution of the solutions. Therefore, investigations were carried out on analogously treated ZIF-8 nanoparticles. Results from solution NMR spectroscopy are depicted in Fig. S8 (ESI†). No signals for the CH_2 or CH_3 group of ethanol can be detected, showing that the material does not contain ethanol anymore. Therefore, such films are considered to be "empty".

The fit of the ellipsometry data also delivers the film thickness. For a sample prepared with three deposition cycles, the film thickness is $d_{3\ \text{cycles}} = 311.6 \pm 18.2$ nm. The values for samples prepared with smaller numbers of cycles are given in Fig. 3 (right, black dots) and show that the total film thickness scales linearly with the number of deposition cycles. Thus, the values for the thicknesses and BET areas of these films show good agreement.

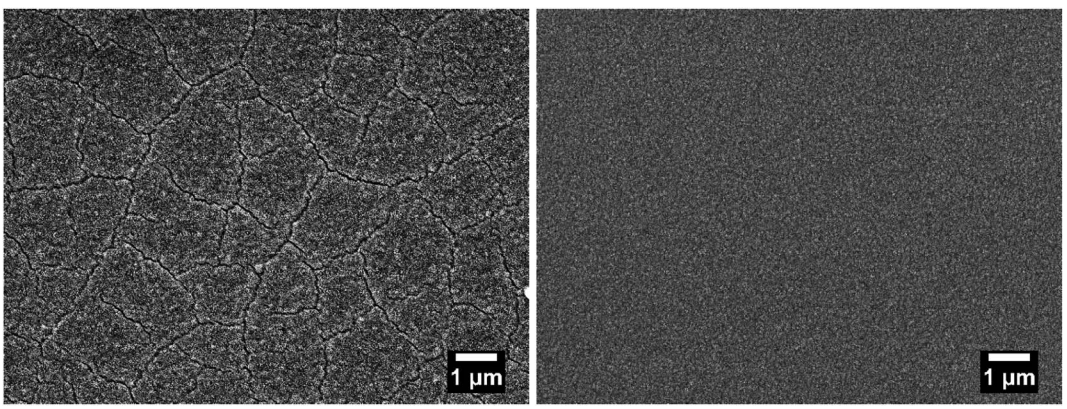

Fig. 2 SEM images of ZIF-8 thin film prepared with (left) and without (right) drying steps between the deposition cycles.

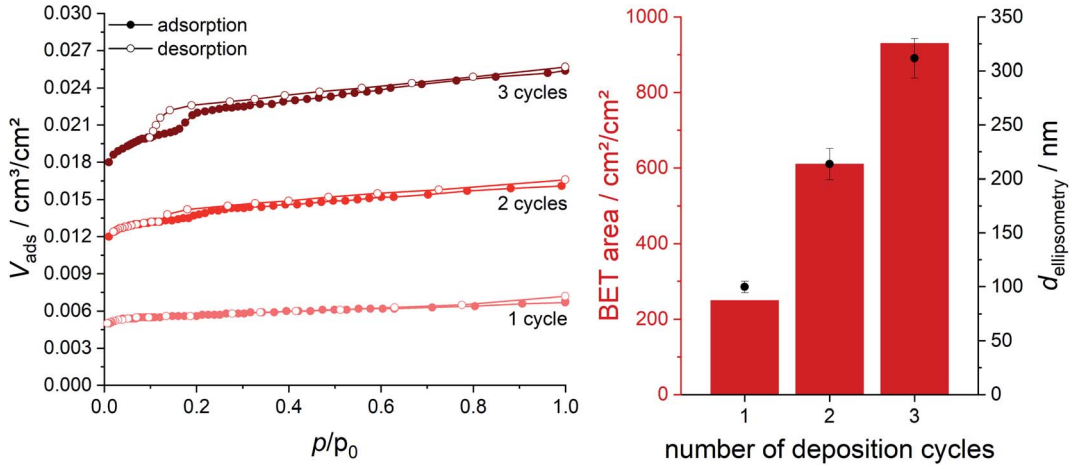

Fig. 3 Krypton physisorption isotherms of ZIF-8 thin films on silicon after 1, 2 and 3 deposition cycles. The resulting BET areas scale linearly with the number of deposition cycles (red columns) as do the film thicknesses which were determined by ellipsometry (black dots).

To investigate the refractive index modulation potential, ZIF-8 films were incubated in different organic media for three days. Again, the refractive indices of several samples were averaged, leading to the refractive indices and refractive index changes reported in Table 1. Also, the refractive index of ZIF-8 after loading with pMA *via* the vapour phase for two days is given in this table.

Loading with these organic compounds enables refractive index tuning in a large range of $\Delta n_{max} = 0.20$. The measured refractive index dispersion curves with standard deviations are shown in Fig. 4. Standard deviations are narrow. The different dispersions are rather regularly distributed over the Δn_{max} range. Thus, the refractive index can be varied in this broad refractive index range by the choice of the loaded guest.

We propose the previously described pore-filling effect[33] as the reason for these large refractive index changes. The refractive indices at room temperature of THF[47] (1.40), DMF[48] (1.43), DMSO[48] (1.48), toluene[49] (1.50), *para*-methyl anisate[50] (1.52) and iodobenzene[51] (1.62) at 589 nm show the same trend that is also visible in the solvent-loaded ZIF-8 thin films. In the pore-filling model the refractive index of the loaded films can be described as a mixed refractive index of the materials components:[33]

$$n_{film} = \sqrt{f_{MOF} n_{MOF}^2 + f_{guest} n_{guest}^2 + (1 - f_{MOF} - f_{guest}) n_{vacuum}^2}$$

f is the volume fraction of each component of the system. The sum of these fractions is 1. Accordingly, the fraction of vacuum is written as $f_{vacuum} = 1 - f_{MOF} - f_{guest}$. Here, "vacuum" designates possible free spaces of the pore system which are not occupied by guest molecules (and possibly those between the grown crystallite which we can, however, not identify in SEM pictures of our samples).

The successful loading was verified with solution ^{1}H-NMR spectroscopy on digested loaded particles (Fig. S8, ESI†) and IR spectroscopy on loaded thin films (Fig. S9, ESI†). Thin films could not be used for the ^{1}H-NMR spectroscopic measurements because of the very low amount of material which was not sufficient to generate signals in the spectrum. The ^{1}H-NMR spectra of samples derived from loaded ZIF-8 particles show additional signals for aromatic protons when they were loaded with pMA, toluene or iodobenzene. Toluene-loaded samples also show an additional peak for the CH_3 group of toluene. For pMA-loaded samples additional signals for the two methyl groups are visible. IR spectra also show additional signals when guests are loaded. The signals are marked in Fig. S9 (ESI†). For

Table 1 Refractive indices and refractive index changes of ZIF-8 films after loading with different molecules

Loaded molecule	n_D	Δn_D
Empty	1.355 ± 0.004	—
Tetrahydrofurane	1.376 ± 0.003	0.02
Dimethylformamide	1.421 ± 0.004	0.07
Dimethylsulfoxide	1.451 ± 0.002	0.10
Toluene	1.481 ± 0.007	0.13
para-Methyl anisate	1.506 ± 0.005	0.15
Iodobenzene	1.552 ± 0.006	0.20

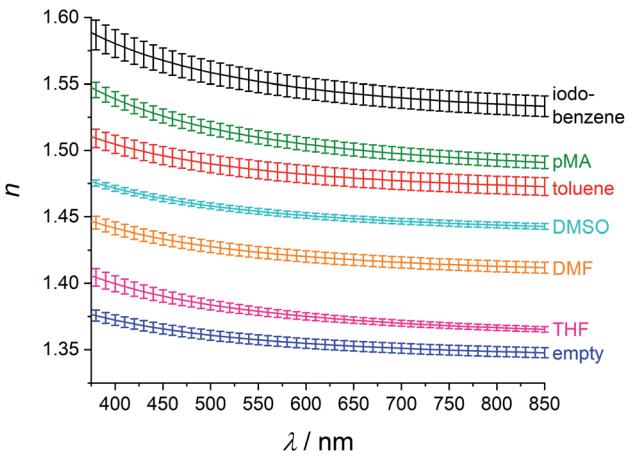

Fig. 4 Refractive index dispersion curves of guest-loaded ZIF-8 films.

all loaded guests, new signals can be found, confirming the successful loading.

To study the processes of loading and exchange of guest molecules more closely, we performed an incubation series of ZIF-8 thin films where the films were incubated alternatively in ethanol and toluene. First, the refractive index of a ZIF-8 film which had been stored in ethanol and which corresponds to the empty pore state was measured by ellipsometry. Afterwards, the film was incubated in toluene for 60 min and the refractive index was determined again. Thereafter, the film was stored in ethanol again for 60 min. This process was alternated three times. The obtained refractive index dispersion curves are shown in Fig. 5. Arrows show the temporal evolution of the refractive index. Incubating the ethanol-soaked thin film in toluene for 60 min leads to a refractive index change $\Delta n_1 = 0.13$. The resulting refractive index shows a good agreement with the previously measured refractive index after three days of incubation in toluene. By incubating the film for 60 min in ethanol, the refractive index does not completely switch back to the value of the empty pore state; however, it can thereafter reversibly be switched repeatedly and reversibly with $\Delta n_{rev} \approx 0.10$ by alternating incubations in toluene and ethanol.

A possible explanation for the incomplete reduction of the refractive index of a toluene-loaded film by a 60 min incubation in ethanol is that the exchange of toluene to ethanol may take longer than the actual exposure time. As a result, some toluene molecules would still remain in the pores. According to the pore-filling model, the refractive index of a partly toluene-loaded ZIF-8 film has to be lower than the refractive index of a toluene-saturated film.

In order to clarify this question, we investigated the exchange kinetics of ethanol and toluene in ZIF-8 thin films in a time-resolved manner using UV/Vis spectroscopy and ellipsometry (Fig. 6). The UV/Vis transmission spectrum of a non-absorbing thin film typically shows interference fringes with minima and maxima depending on the films' thickness and on its refractive index. Changes in the refractive index can be monitored by a shift of the transmission maxima and minima. First, an ethanol-soaked ZIF-8 film was incubated in toluene (see Fig. 6a). With increasing incubation time, the transmission maximum in the UV/Vis spectra shifts to higher wavelength. Such a red shift is typical for a refractive index increase and confirms the refractive index change that was measured with ellipsometry. After 60 min no significant further shift takes place. The total shift is $\Delta\lambda = 68$ nm. This result shows a good agreement with analogue ellipsometry measurements (see Fig. 6c). There, the refractive index increases rapidly in the beginning and reaches the refractive index of the toluene-loaded ZIF-8 thin films with long incubation times after 60 minutes. Thus, the pores in a ZIF-8 film can be filled with toluene within 60 min. In a second experiment the removal of toluene was investigated. For this, a toluene saturated ZIF-8 film was incubated in ethanol (see Fig. 6b). Again, the UV/Vis transmission spectra were measured in a time-resolved manner. With increasing incubation time, the transmission maximum shows a blue shift which is typical for a refractive index decrease. The total shift is $\Delta\lambda = 69$ nm. In this case, the process needs more time: only after 180 min, no further shift takes place. This explains why within the experiments depicted in Fig. 5, the refractive index does not return to the value observed before toluene loading after only 60 min of ethanol incubation. Also, the results of this experiment were confirmed by ellipsometry (see Fig. 6d). The refractive index decreases when the film is incubated in ethanol. After 180 min, the refractive index reaches the same value as for an empty ZIF-8 thin film. This offers the possibility of fine-tuning the refractive index by either partly filling the MOF or by filling it with mixtures of guests.

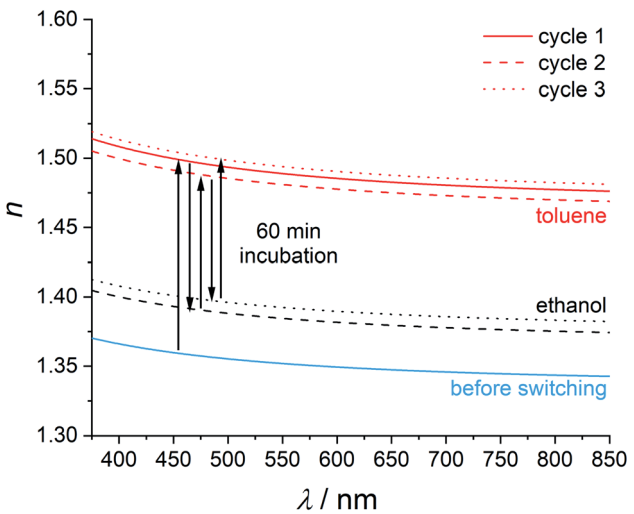

Fig. 5 Refractive index switching as determined by ellipsometry measurements in ZIF-8 films with ethanol and toluene. The arrows should be read from left to right to follow the chronological evolution of the refractive index in this experiment.

Pore-filling cannot only be achieved from the liquid but also from the vapour phase. In corresponding experiments, we used argon as the feed gas and saturated the argon flow by passing it through ethanol. We first carried out a reference experiment with a sample consisting of a silica layer with *ca.* 100 nm thickness on a silicon wafer (for the results see the ESI, Fig. S10†). No effect of the argon or argon/ethanol flow on the refractive index can be seen in this reference experiment. The measured refractive index shows good agreement with the refractive index of silica (1.46).[52]

The refractive index of ZIF-8 is stable under exposure to argon. When the argon flow passes through ethanol, the refractive index of the ZIF-8 thin film directly increases with $\Delta n = 0.12$ and stabilises within a few minutes. When the gas flow is changed to pure argon, the refractive index directly decreases ($\Delta n = 0.11$). This process can be cycled and shows a reversible refractive index change of approximately 0.11 (Fig. 7). The large refractive index changes with high reversibility can be explained by the weak interaction between ethanol and ZIF-8 which has also been shown by ^{1}H-NMR spectroscopy (Fig. S8, ESI†). This experiment also shows that switching *via* the gas phase is fast. In addition, we have performed fast UV/Vis measurements to get more insight into the kinetics of this process (see ESI,

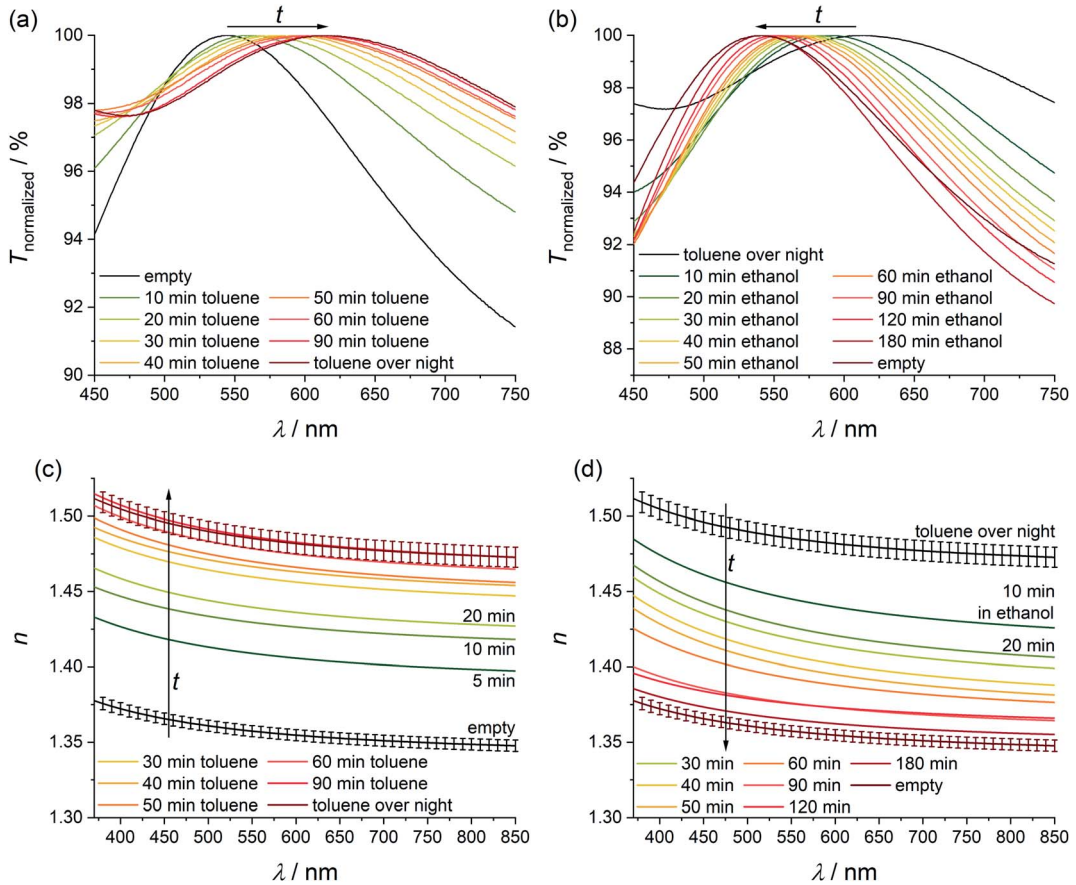

Fig. 6 UV/Vis (a and b) and ellipsometry (c and d) studies on the kinetics of the loading of an empty ZIF-8 thin film with toluene (a and c) and on the kinetics of the removal of toluene from the pores by incubation in ethanol (b and d).

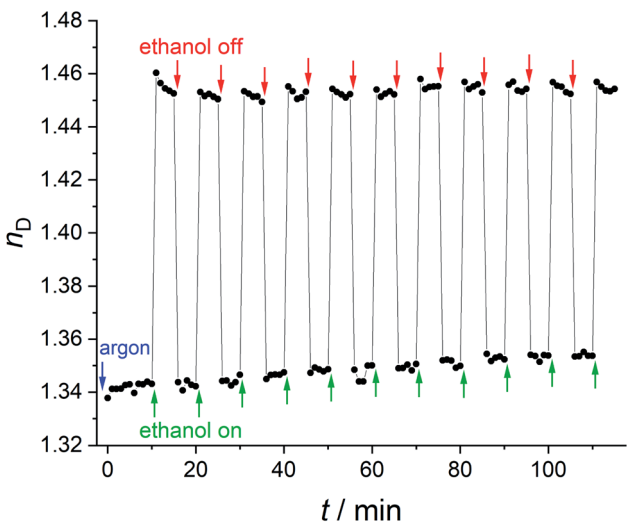

Fig. 7 Refractive index switching of a ZIF-8 thin film with ethanol *via* the gas phase.

Fig. S11† for the results and for the description of the experiment). We cannot discern any delay for the switching using our experimental set-up. The time resolution limit of these measurements is eight seconds, so we can state that the switching is complete after eight seconds, but may also be faster. For most optical applications which benefit from a change of the refractive index, this should be of advantage.[53]

4. Conclusion

In this work we have shown that very large refractive index changes can be achieved by using the metal–organic framework ZIF-8 as a host structure for different organic guest molecules. The resulting refractive index can be fine-tuned in a wide range of $\Delta n \approx 0.20$. The refractive index changes can be explained by the pore-filling model. Refractive index modulation can also be performed partly and reversibly by alternated incubation of ZIF-8 thin films in ethanol and toluene. Finally, we showed that fast refractive index switching is possible *via* the gas phase with a switching time of eight seconds or less, which is much faster than a refractive index change of comparable size in a MOF thin film consisting of HKUST-1.[30]

For the experiments carried out, ZIF-8 thin films of high optical quality were necessary. Therefore, the method of cycled direct crystallization was preferred over nanoparticle deposition. This method was further advanced by modifying the described synthesis protocol,[37] showing that by neglecting drying steps, crack-free thin films with high optical quality can

be obtained. In spite of the renunciation of the drying steps, crystalline films were obtained.

Large refractive index changes which can be influenced externally can be useful, for example, in the construction of photonic crystals and optical filters.[54] Filling the pores only partially leads to index changes sufficient for many optical devices (Δn typically 0.02 to 0.03). Large refractive index changes are preferred for sensor materials, as they provide high sensitivities, *i.e.* when only very low degrees of filling translate to measurable index changes.

Conflicts of interest

To the best of their knowledge, the authors declare no conflict of interests.

Acknowledgements

This work is funded by the Deutsche Forschungsgemeinschaft (DFG) under Germany's Excellence Strategy within the Cluster of Excellence PhoenixD (EXC 2122, Project ID 390833453). Karen Hindricks thanks the the Studienstiftung des Deutschen Volkes (German National Academic Foundation) for a scholarship. The authors like to thank Hendrik A. Schulze (ACI, Leibniz University Hannover) for support in the early stages of this work. We also want to thank Sebastian Bengsch (IMPT, Leibniz University Hannover) for providing and cutting silicon wafers and Lars Klepzig (PCI, Leibniz University Hannover) for useful discussions. Our thanks also go to the NMR department of the Institute for Organic Chemistry at the Leibniz University Hannover.

References

1 Y. Fan, T. Zhu, L. Shi and Y.-J. Rao, *Appl. Opt.*, 2011, **50**, 4604–4610.
2 T. Höfler, T. Grießer, X. Gstrein, G. Trimmel, G. Jakopic and W. Kern, *Polymer*, 2007, 1930–1939.
3 G. L. Li and P. Yu, *J. Lightwave Technol.*, 2003, **21**, 2010–2030.
4 G. Langer, T. Kavc, W. Kern, G. Kranzelbinder and E. Toussaere, *Macromol. Chem. Phys.*, 2001, **18**, 3459–3467.
5 B. Chmielak, M. Waldow, C. Matheisen, C. Ripperda, J. Bolten, T. Wahlbrink, M. Nagel, F. Merget and H. Kurz, *Opt. Express*, 2011, **19**, 17212–17219.
6 O. Solgaard, A. A. Godil, R. T. Howe, L. P. Lee, Y.-A. Peter and H. Zappe, *J. Microelectromech. Syst.*, 2014, **3**, 517–538.
7 L. Novak, P. Neuzil, J. Pipper, Y. Zhang and S. Lee, *Lab Chip*, 2007, **7**, 27–29.
8 B. Panella and M. Hirscher, *Adv. Mater.*, 2005, **5**, 538–541.
9 M. Woellner, S. Hausdorf, N. Klein, P. Mueller, M. W. Smith and S. Kaskel, *Adv. Mater.*, 2018, **30**, e1704679.
10 M. D. Allendorf, R. Dong, X. Feng, S. Kaskel, D. Matoga and V. Stavila, *Chem. Rev.*, 2020, **120**, 8581–8640.
11 A. H. Chughtai, N. Ahmad, H. A. Younus, A. Laypkov and F. Verpoort, *Chem. Soc. Rev.*, 2015, **44**, 6804–6849.
12 C. A. Trickett, A. Helal, B. A. Al-Maythalony, Z. H. Yamani, K. E. Cordova and O. M. Yaghi, *Nat. Rev. Mater.*, 2017, **2**, 17045.
13 D. Gygi, E. D. Bloch, J. A. Mason, M. R. Hudson, M. I. Gonzalez, R. L. Siegelman, T. A. Darwish, W. L. Queen, C. M. Brown and J. R. Long, *Chem. Mater.*, 2016, **28**, 1128–1138.
14 Y. Ji, L. Ding, Y. Cheng, H. Zhou, S. Yang, F. Li and Y. Li, *J. Phys. Chem. C*, 2017, **121**, 24104–24113.
15 X. Yang and Q. Xu, *Cryst. Growth Des.*, 2017, **17**, 1450–1455.
16 U. Böhme, B. Barth, C. Paula, A. Kuhnt, W. Schwieger, A. Mundstock, J. Caro and M. Hartmann, *Langmuir*, 2013, **29**, 8592–8600.
17 L. Fan, Z. Kang, Y. Shen, S. Wang, H. Zhao, H. Sun, X. Hu, H. Sun, R. Wang and D. Sun, *Cryst. Growth Des.*, 2018, **18**, 4365–4371.
18 A. Knebel, B. Geppert, K. Volgmann, D. I. Kolokolov, A. G. Stepanov, J. Twiefel, P. Heitjans, D. Volkmer and J. Caro, *Science*, 2017, **358**, 347–351.
19 O. Shekhah, J. Liu, R. A. Fischer and C. Wöll, *Chem. Soc. Rev.*, 2011, **40**, 1081.
20 I. Stassen, N. Burtch, A. Talin, P. Falcaro, M. Allendorf and R. Ameloot, *Chem. Soc. Rev.*, 2017, **46**, 3185–3241.
21 J. F. Olorunyomi, S. T. Geh, R. A. Caruso and C. M. Doherty, *Mater. Horiz.*, 2021, **8**, 2387.
22 Z.-G. Gu, A. Pfriem, S. Hamsch, H. Breitwieser, J. Wohlgemuth, L. Heinke, H. Gliemann and C. Wöll, *Microporous Mesoporous Mater.*, 2015, 82–87.
23 W. Yin, C. Tao, F. Wang, J. Huang, T. Qu and J. Wang, *Sci. China Mater.*, 2018, **61**, 391–400.
24 Y. Huang, C. Tao, R. Chen, L. Sheng and J. Wang, *Nanomaterials*, 2018, **8**, 676.
25 W. Vandezande, K. P. F. Janssen, F. Delport, R. Ameloot, D. E. de Vos, J. Lammertyn and M. B. J. Roeffaers, *Anal. Chem.*, 2017, **89**, 4480–4487.
26 K.-J. Kim, P. Lu, J. T. Culp and P. R. Ohodnicki, *ACS Sens.*, 2018, **3**, 386–394.
27 A. Demessence, C. Boissière, D. Grosso, P. Horcajada, C. Serre, G. Férey, G. J. A. A. Soler-Illia and C. Sanchez, *J. Mater. Chem.*, 2010, **20**, 7676.
28 O. Dalstein, D. R. Ceratti, C. Boissière, D. Grosso, A. Cattoni and M. Faustini, *Adv. Funct. Mater.*, 2016, **26**, 81–90.
29 P. Horcajada, C. Serre, D. Grosso, C. Boissière, S. Perruchas, C. Sanchez and G. Férey, *Adv. Mater.*, 2009, **21**, 1931–1935.
30 E. Redel, Z. Wang, S. Walheim, J. Liu, H. Gliemann and C. Wöll, *Appl. Phys. Lett.*, 2013, **103**, 91903.
31 W. Yin, C. Tao, X. Zou, F. Wang, T. Qu and J. Wang, *Nanomaterials*, 2017, **7**, 242.
32 M. C. So, S. Jin, H.-J. Son, G. P. Wiederrecht, O. K. Farha and J. T. Hupp, *J. Am. Chem. Soc.*, 2013, **135**, 15698–15701.
33 G. Lu, O. K. Farha, L. E. Kreno, P. M. Schoenecker, K. S. Walton, R. P. van Duyne and J. T. Hupp, *Adv. Mater.*, 2011, **23**, 4449–4452.
34 Y. Wu, F. Li, W. Zhu, J. Cui, C. Tao, C. Lin, P. M. Hannam and G. Li, *Angew. Chem., Int. Ed.*, 2011, **50**, 12518–12522.

35 C. Bartual-Murgui, A. Akou, C. Thibault, G. Molnár, C. Vieu, L. Salmon and A. Bousseksou, *J. Mater. Chem. C*, 2015, **3**, 1277–1285.
36 L. Li, X. Jiao, D. Chen, B. V. Lotsch and C. Li, *Chem. Mater.*, 2015, **27**, 7601–7609.
37 G. Lu and J. T. Hupp, *J. Am. Chem. Soc.*, 2010, **132**, 7832–7833.
38 K. S. Park, Z. Ni, A. P. Côté, J. Y. Choi, R. Huang, F. J. Uribe-Romo, H. K. Chae, M. O'Keeffe and O. M. Yaghi, *Proc. Natl. Acad. Sci. U. S. A.*, 2006, **103**, 10186–10191.
39 A. Phan, C. J. Doonan, F. J. Uribe-Romo, C. B. Knobler, M. O'Keeffe and O. M. Yaghi, *Acc. Chem. Res.*, 2010, **43**, 58–67.
40 D. Saliba, M. Ammar, M. Rammal, M. Al-Ghoul and M. Hmadeh, *J. Am. Chem. Soc.*, 2018, **140**, 1812–1823.
41 I. Stassen, M. Styles, G. Grenci, H. van Gorp, W. Vanderlinden, S. D. Feyter, P. Falcaro, D. D. Vos, P. Vereecken and R. Ameloot, *Nat. Mater.*, 2016, **15**, 304–310.
42 M. Tu, H. Reinsch, S. Rodríguez-Hermida, R. Verbeke, T. Stassin, W. Egger, M. Dickmann, B. Dieu, J. Hofkens, I. F. J. Vankelecom, N. Stock and R. Ameloot, *Angew. Chem., Int. Ed.*, 2019, **58**, 2423–2427.
43 S. Kedenburg, M. Vieweg, T. Gissibl and H. Giessen, *Opt. Mater. Express*, 2012, **11**, 1588.
44 K. Moutzouris, M. Papamichael, S. C. Betsis, I. Stavrakas, G. Hloupis and D. Triantis, *Appl. Phys. B*, 2014, **116**, 617–622.
45 J. Tao, X. Wang, T. Sun, H. Cai, Y. Wang, T. Lin, D. Fu, L. L. Y. Ting, Y. Gu and D. Zhao, *Sci. Rep.*, 2017, **7**, 41640.
46 E. Santanach Carreras, F. Chabert, D. E. Dunstan and G. V. Franks, *J. Colloid Interface Sci.*, 2007, **313**, 160–168.
47 H.-C. Ku, C.-C. Wang and C.-H. Tu, *J. Chem. Eng. Data*, 2008, **53**, 566–573.
48 K. Moodley, T. Chetty and D. Ramjugernath, *J. Chem. Eng. Data*, 2019, **64**, 3367–3374.
49 F.-H. Hu, L.-S. Wang and S.-F. Cai, *J. Chem. Eng. Data*, 2010, **55**, 492–495.
50 https://www.chemicalbook.com/ChemicalProductProperty_DE_CB5189041.htm.
51 M. G. Voronkov, N. N. Vlasova, L. I. Belousova, A. V. Vlasov, T. I. Vakul'skaya, G. F. Prozorova and S. S. Khutsishvili, *Russ. J. Org. Chem.*, 2013, **49**, 17–21.
52 D. Lo, L. Shi, J. Wang, G.-X. Zhang and X. Zhu, *Appl. Phys. Lett.*, 2002, **81**, 2707–2709.
53 S. Mias and H. Camon, *J. Micromech. Microeng.*, 2008, **18**, 83002.
54 P. Chen, D. He, Y. Jin, J. Chen, J. Zhao, J. Xu, Y. Zhang, F. Kong and H. He, *Opt. Express*, 2018, **26**, 157–164.